CrossMark

Structure and thermal properties of decanoic acid/expanded graphite composite phase change materials

Yuntao Li[1] · Hua Yan[1] · Qun Wang[1] · Hongtao Wang[1] · Yongbo Huang[2]

Abstract Decanoic acid/expanded graphite composite phase change materials (DA/EG-PCMs) with high stability and excellent thermal conductivity were fabricated by blending expanded graphite (EG) and decanoic acid (DA). The structure, thermo-physical properties, and the formation mechanism of DA/EG-PCMs were investigated. The obtained results demonstrate that EG exhibits a network-like porous structure, which is superimposed of 10–50 μm thick graphite sheet. Therefore, DA can be effectively encapsulated through the binding between micropores and the surface adsorption of EG resulting in a relatively smaller DA/EG-PCMs particle with better dispersibility. In addition, adding EG into DA also increased both the thermal stability and the thermal conductivity while decreasing the charging and discharging time, which resulted in improved thermal efficiencies. Although adding EG can negatively influence the phase change behavior of DA, the temperature and enthalpy of phase change were still as high as 34.9 °C and 153.1 J g^{-1}, respectively. Based on a combination of experimental results and a comprehensive analysis of the phase transformation kinetics, it is concluded that DA/EG-PCMs with 10 mass% EG with improved thermal properties can meet the requirements for efficient temperature control in low-to-medium environments.

Introduction

The phase change technology is an important aspect in studies dealing with energy conservation and emission reduction, and this has provided a potent impetus for the development of new materials. PCM (phase change material) is considered to be a type of renewable energy material with high energy utilization efficiency [1, 2]. PCMs control the temperature of a system by absorbing and releasing heat during phase change. In view of their high thermal storage densities and the capacity to maintain a constant temperature during endothermic and exothermic processes, PCMs have extensive applications in energy saving as applied to buildings, industrial waste heat storage and recycling, solar energy utilization and infrared camouflage in military applications [3–5].

Currently, research efforts are focused on the improvement of the thermal properties of PCM, especially in regard to composite phase change materials (CPCM) [6–8]. Zhang [9] prepared a paraffin/expanded graphite CPCM where paraffin served as the phase change material and expanded graphite was used as the supporting structure. Shi [10] prepared paraffin/attapulgite CPCM that had the adsorption properties of attapulgite and measured the thermal physical properties of the composite. Fleischer [11] reported that carbon-based nanoparticles drastically 6reduced the phase change time of PCM when compared to Al/paraffin and TiO$_2$/paraffin nanocomposites. Jia [12] prepared a stearic acid/SiO$_2$ form-stable and shape-stabilized CPCM by means of an ultrasound assisted sol–gel process with stearic acid functioning as the phase change group. Trigui [13] used

✉ Hua Yan
  Yuntao Li
  1026774457@qq.com

[1] Department of Chemistry and Material Engineering, Logistical Engineering University, Chongqing 401311, China

[2] College of Materials Science and Engineering, Chongqing University, Chongqing 400045, China

LDPE as a supporting matrix in a LDPE/wax composite PCM, which demonstrated a good potential for application in passive solar walls. Using a self-polymerization method, Wang [14] prepared the fatty acid eutectic/polymethyl methacrylate composite as a form-stable PCM for thermal energy storage. Li [15] reported on the stable properties of EG/$Na_2S_2O_3\cdot 5H_2O$ phase change energy storage composite by adding the nucleating agent K_2SO_4, calcium sulphate dihydrate ($Ca_2SO_4\cdot 2H_2O$), tetrasodium pyrophosphate decahydrate ($Na_4P_2O_7\cdot 10H_2O$) and enhance heat transfer material expanded graphite (EG) could improve the performance. Sari [16, 17] tested a series of eutectic mixtures of selected fatty acids for thermal reliability. According to previous studies, the possible ways to improve the thermal properties of PCMs are the following: Inserting fins or tubes of different configurations into PCM, impregnating liquid PCM into high thermal conductivity porous materials, employing multiple PCMs, or packing PCMs using micro-encapsulation. In summary, while previous studies have concentrated more on the preparation process parameters and the methods to improve thermal properties, no comprehensive study has yet been carried out on the structure, mechanism, and stability of CPCM as applied to its application in the temperature control of low-to-medium temperature environments, especially by way of phase transformation kinetics and experimental results.

Decanoic acid (DA), a typical PCM with excellent properties, has a low phase transition temperature, high latent heat and does not corrode. Hence, it is appropriate for an investigation of the temperature control in a low-to-medium temperature environment. However, disadvantages such as low thermal conductivity and thermal stability, and a low rate of heat transmission, adversely affect the temperature control efficiency [18]. In addition, DA is a liquid above the phase change temperature [19] and therefore, it is important to choose a suitable substrate packaging material to overcome these disadvantages so as to enhance the stability of DA during temperature control [20]. Expanded graphite (EG) is natural flake graphite that can rapidly expand at high temperatures. EG has a high thermal conductivity similar to natural graphite, a large specific surface area, and good adsorption properties. Due to its excellent properties such as high stability, high thermal conductivity, good compatibility with organic PCMs, and a lower density and mass when compared to metal promoters [21], EG is considered to be an appropriate PCM packaging material to surmount problems related to DA.

To better understand the structure and mechanism of CPCM and to develop stable CPCMs with excellent thermal properties, in this study, decanoic acid/expanded graphite composite phase change materials (DA/EG-PCMs) were prepared using the melt-blending method, by combining EG that has a high thermal conductivity and good adsorption properties, with DA. The goal of this work is to analyze the structure, mechanism, stability, thermal properties and phase change behavior in DA/EG-PCMs by means of phase transformation kinetics and experiments, and to comprehensively determine the optimal proportion of DA and EG in DA/EG-PCMs. The DA/EG-PCMs are expected to show good potential for application in the temperature control of low-to-medium temperature environments, and hence, it is of great significance to develop and bring in innovative modifications to the existing phase technology.

Materials and methods

Materials

DA (phase change temperature: 33–36 °C and phase change enthalpy: 160–175 kJ kg^{-1}) was supplied by Shanghai Jingchun Biological&Chmical Co., Ltd. China. EG (expansion ratio: 210 mL g^{-1}, 180 μm size) was provided by Qingdao Jirilai Graphite Co., Ltd. China.
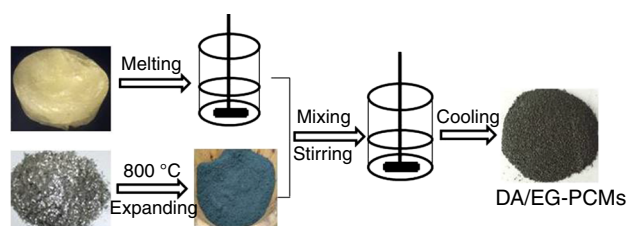
Preparation of DA/EG-PCMs

Preparation of EG: 1.8 g of flake graphite was heated in a furnace at 800 °C for 20 s. After rapid cooling in air, expanded graphite with a volume expansion of 210 mL/g was obtained.

Preparation of DA/EG-PCMs: DA is heated using a KDM heating sleeve at 80 °C so as to melt it completely. EG is added into the DA melt and stirred to form a homogeneous mixture. After rapid cooling in air, DA/EG-PCMs are obtained. The percent of EG in DA/EG-PCMs are 0, 5, 10, 15 and 20 mass%, respectively. The corresponding DA/EG-PCMs with different compositions are labeled as C1, C2, C3, C4, and C5, respectively, a schematic diagram of the preparation is shown in Fig. 1.

Methods

The microstructure of DA/EG-PCMs was investigated by SEM (S-3700N, Hitachi, Japan) at a voltage of 20 kV and with a high-resolution image quality.

Fig. 1 Scheme of the process for the preparation of DA/EG-PCMs

Thermogravimetric analysis was conducted using a Netzsch STA449C thermal analyzer (heating rate: 10 °C/min, measurement temperature range 30–400 °C).

To analyze the phase changes in DA/EG-PCMs, differential scanning calorimetry (404 F3 DSC) was performed in N_2 atmosphere in the temperature range 30–80 °C at three different heating rates (3, 5 and 8 °C min^{-1}).

IR spectra were taken using a Nicolet 6700 FT-IR spectrophotometer to study the chemical structure of DA/EG-PCMs. A total of 32 scans were taken in the range of 4000–40 cm^{-1}.

The thermal conductivity tester DRE-2C was employed to measure the thermal conductivity of DA/EG-PCMs. The measurement range was from 0.01 to 100 W/(mK), and the specimen was prepared in a mold with 50 mm diameter and 20 mm height (Fig. 2a).

Test to evaluate the ability to store and release heat: Equal volumes of DA and DA/EG-PCMs were added into 5 tubes, and these were placed in a test tube maintained at 70 °C that served as a constant temperature with water bath. The tubes were quickly removed from the bath into ambient temperature (25 °C), and the changes in the sample temperature were recorded at intervals of 10 s using a RC-4 temperature recorder. (Fig. 2b).

The thermal cycling stability test: DA/EG-PCMs of a certain shape were taken and placed on a filter paper and heated to 100 °C in an electro-thermal blowing dry box. The sample was cooled down to 25 °C and heating and cooling cycle was repeated 20 times. At the end of the experiment, the mass loss, thermal efficiency, and configurational changes of DA/EG-PCMs were compared before and after thermal cycling.
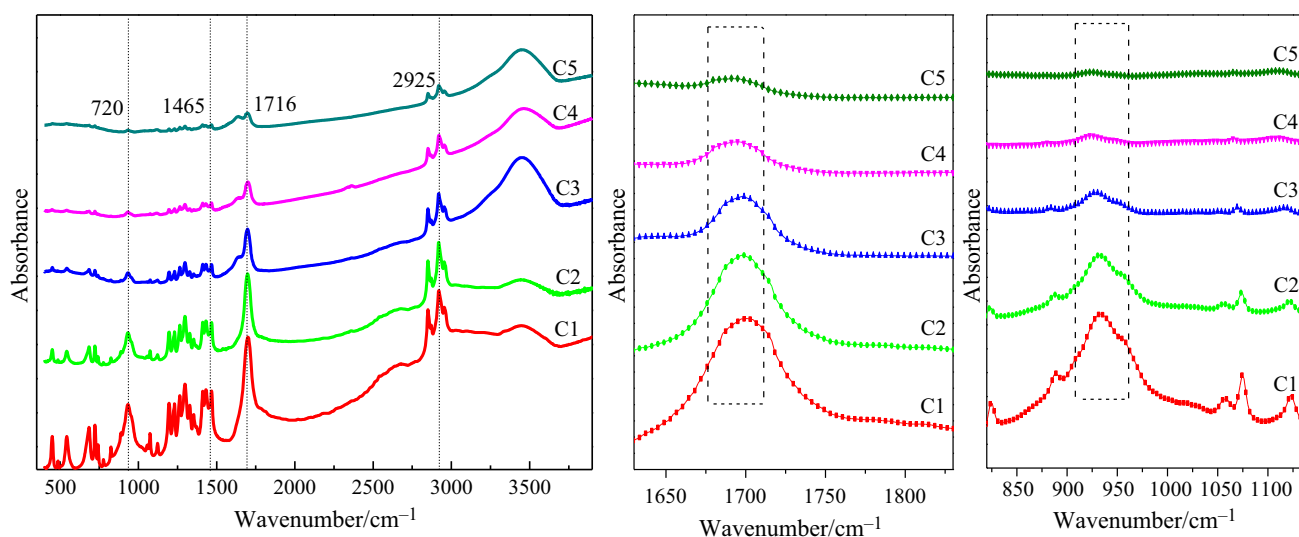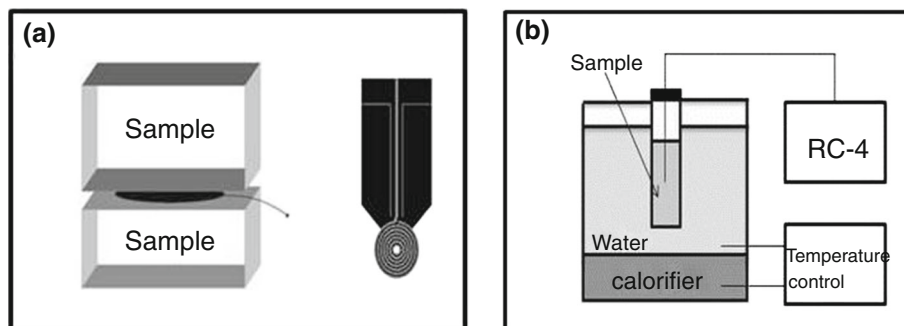
Results and discussion

Morphology of DA/EG-PCMs

Structures of DA/EG-PCMs

The chemical structure of DA/EG-PCMs is elucidated from IR spectra shown in Fig. 3. Two intense absorption peaks at 2925 and 1465 cm^{-1} attributed to C–H stretching


Fig. 2 A schematic diagram of test

Fig. 3 FT-IR spectra of pure DA and DA/EG-PCMs

vibrations (Vs) and C–H in-plane bending vibrations (δ), respectively, are observed. The infrared spectra also show the –OH in-plane (δ) and out of plane bending vibrations (Y) at 1430 and 940 cm^{-1}, respectively. The peak at 1716 cm^{-1} corresponds to the C=O stretching vibration, showing that DA exists mainly in the form of a dimer. The absorption band at 720 cm^{-1} is assigned to the in-plane C–H bending vibration and the in-plane deformation rocking vibration of DA molecule. The characteristic absorption peaks are in good agreement with those observed in the IR of pure DA [22]. However, the spectral intensity is lower due to the capping effect of EG. Also, the peak widths of –OH bending vibrations at 940 cm^{-1} increase and the C=O stretching vibration shift from 1720 to 1700 cm^{-1}, it is concluded that the hydrogen bond forms between DA and EG. Furthermore, it is indicated that in the DA/EG-PCMs, DA and EG are bonded to each other by physical forces, namely, hydrogen bonding, without the formation of a new compound by chemical bonding. Therefore, the composite DA/EG-PCMs retain the good thermal performance of DA and the thermal stability of EG [23].

Morphology and mechanism of DA/EG-PCMs

Figure 4 shows the optical image and micrographs of EG and DA/EG-PCMs, respectively. EG is a crystalline mineral made of carbon, and has a hexagonal layered structure. The distance between the layers is ~ 340 pm, and the layers are held by Van der Waals forces. SEM images show the structure of EG: wormlike appearance structure, worm wrapping space and internal space. There are a large number of microvoids, constituted by parallel and collapsed layers which are piled up with graphite lamination of micrometer. Therefore, EG has excellent adsorption properties and provides sufficient space to encapsulate DA, as shown in Fig. 4a. From Fig. 4b, it can be seen that the surface of EG becomes smooth after adsorbing DA into the microvoids. When the EG content is 5 mass%, the amount of DA is higher than the adsorption capacity of EG, and this results in a large amount of DA remaining on the surface that forms a bulky mass. When the EG content exceeds 10 mass%, the DA/EG-PCMs particles resemble small balls of uniform sizes, with smooth surfaces with no obvious surface in homogeneities such as pits, and without

Fig. 4 a Molecule structure, SEM images and optical image of EG b SEM images of DA/EG-PCMs c optical image of DA/EG-PCMs
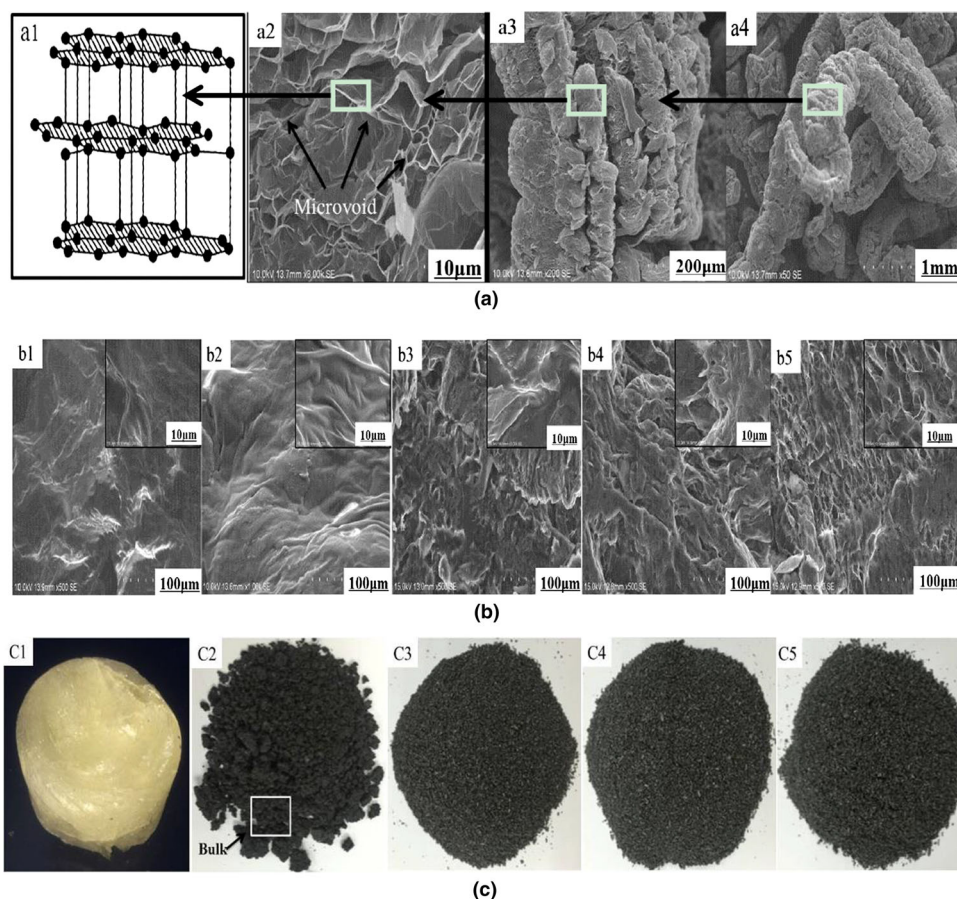
massive bulk and large area thin layer of organic matter [24] (Fig. 4c). Hence, it is concluded that DA/EG-PCMs with 10 mass% of EG are likely to be well encapsulated.

From Figs. 5 and 6, it is observed that hydrogen bonds are formed between the surface functional groups (–O–O–, –C=O and –C–O–) of EG [25] and the molecular chains of DA. The structure, surface properties (surface polarity, surface oxygen groups and specific surface area) of EG and the hydrogen bonds jointly inhibit the movement of the molecular chains of DA by thermal diffusion. In addition, the confined space formed by the micron-sized voids in EG also hinders this movement due to thermal diffusion. These observations indicate that micropore binding and surface adsorption, ensure that DA is both encapsulated and dispersed (Table 1). Furthermore, the combination of DA and EG effectively solves the problem of leakage and overflow of DA at the phase transition temperature. From the above observations, it is clear that DA/EG-PCMs retain the stability and solid particles due to micropore binding and surface adsorption, which facilitates its mixing with other materials.

Phase change properties of DA/EG-PCMs

Temperature and enthalpy of phase change

DSC curves have been plotted to investigate the phase transition behavior and properties of DA/EG-PCMs. The initial phase change temperature (T_0), the melting-peak temperature (T_p) and the phase change enthalpy (H_m) of DA/EG-PCMs at different heating rates are shown in Fig. 7. The endotherm ~ 37 °C corresponds to the phase change in DA upon heat absorption. With increase of heating rate, the endotherms show an obvious shift toward higher temperatures due to the delayed heat transfer of DA under the high heating rate, which inhibits the molecular chains of DA from separating from the crystalline. With increase in EG content, the T_0 of DA/EG-PCMs decreases;
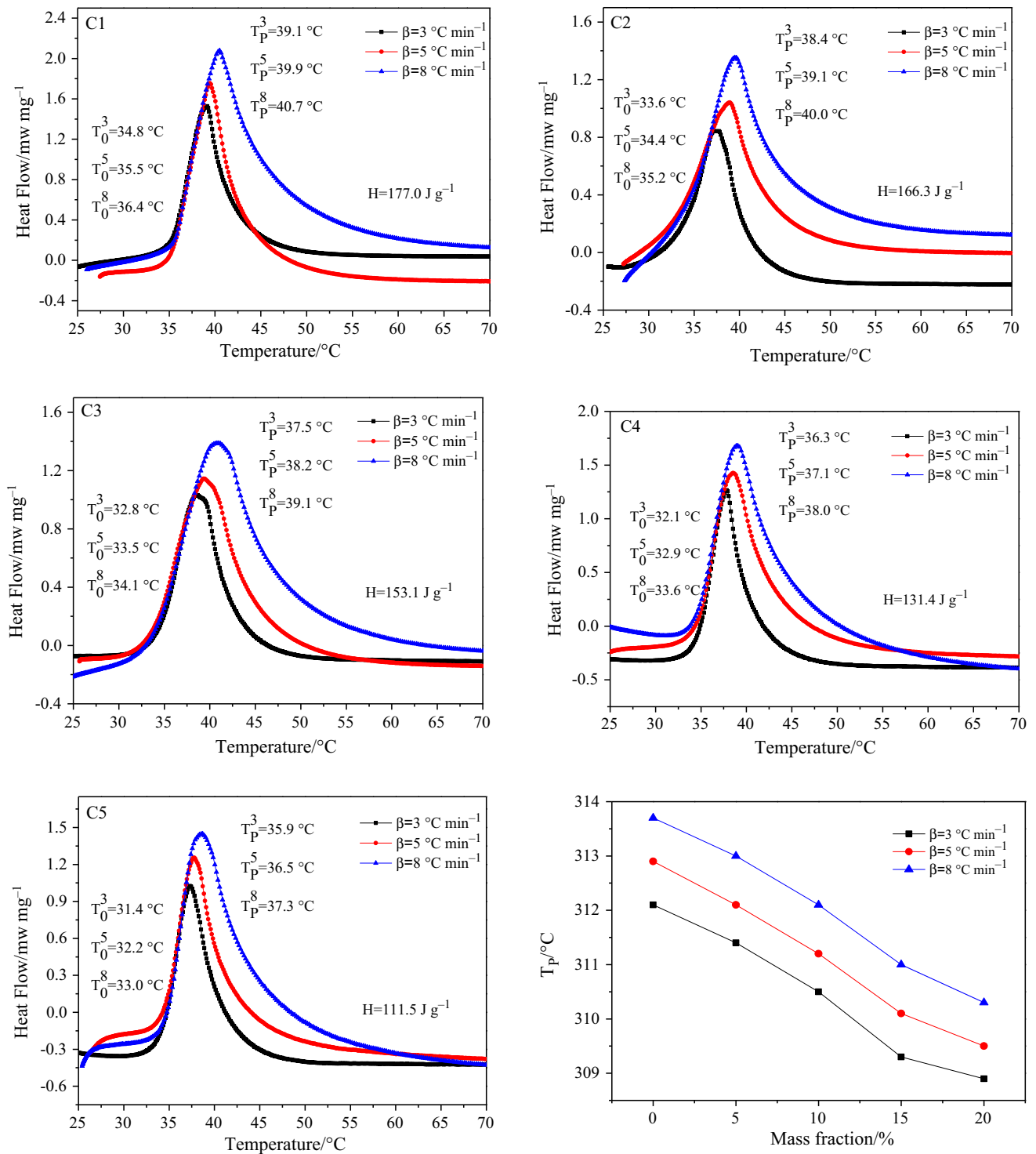

Fig. 5 EDS spectrogram of EG

Element	Mass%	At%
··CK	97.87	98.39
··OK	02.13	01.61
Matrix	Correction	ZAF
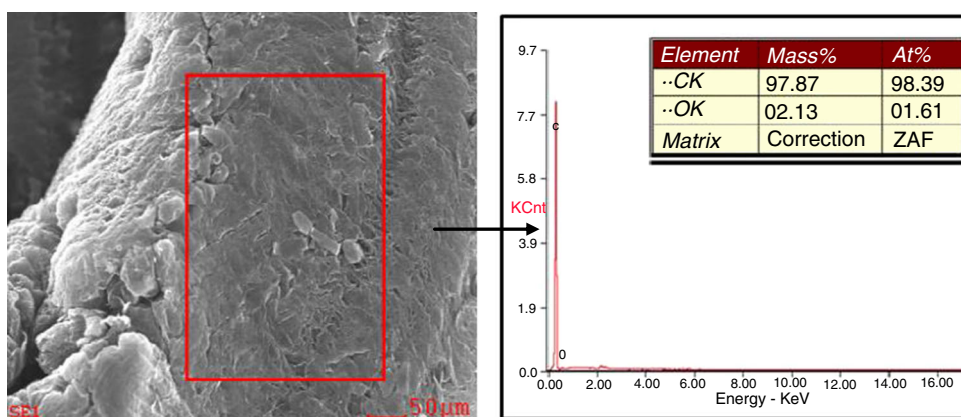
Fig. 6 Schematic of the interaction of DA with EG
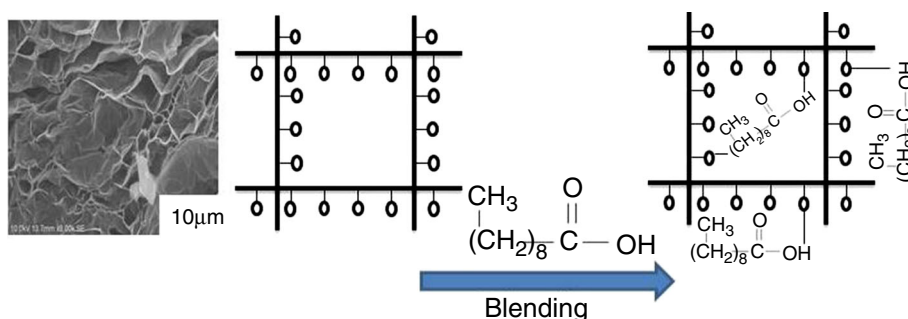
Table 1 The interactions of DA with EG

Influence factor	Micropore binding	Surface adsorption		
		Specific surface area	Surface polarity	Hydrogen bond
DA/EG-PCMs	√	√	√	√

Fig. 7 DSC curves and T_P of DA/EG-PCMs at different heating rates

this is attributed to the high thermal conductivity EG, which in turn enhances the thermal conductivity of DA/EG-PCMs [21]. Therefore, sufficient heat can be absorbed at a relatively lower temperature to bring about the phase change.

The phase change enthalpy is also an important parameter that determines the thermal properties of CPCM. The addition of EG into DA results in a relatively lower phase change enthalpy (H_m), which decreases gradually with increase in EG content. On one hand, the addition of

EG is at the expense of DA in DA/EG-PCMs, and the phase change enthalpy of the composite system is solely determined by DA as there is no phase change of EG at these low temperatures. On the other hand, the interaction between DA and EG changes the molecular arrangement and free energy of DA/EG-PCMs, leading to a change in thermal properties. Furthermore, the above conclusion can be verified by the theory of mixtures [26]. Thus, the phase change enthalpy of DA/EG-PCMs can be calculated from the following equation.

$$\Delta H_C = (1 - \varphi)\Delta H_m \tag{1}$$

Where ΔH_c (J g^{-1}) is the latent heat of DA/EG-PCMs, ΔH_m (J g^{-1}) is the latent heat of pure DA, and Φ is the mass fraction of EG. The H_m of DA/EG-PCMs is approximately equal to that of DA, and this decreases with increase in EG content. When the EG content exceeds 10 mass%, a more significant reduction in H_m can be observed. In addition, the phase change enthalpy of DA/EG-PCMs is $\sim$78.7% of the theoretical value when the EG content is 20 mass%.

Phase transformation kinetics

According to the phase transformation kinetics theory detailed in previous reports [27], we can know the followings.

Phase transformation kinetics equation

$$\frac{d\alpha}{dt} = Ae^{-E/RT}(1 - \alpha)^n \tag{2}$$

Differential to Eq. (2)

$$\frac{d}{dt}\left[\frac{d\alpha}{dt}\right] = \left[A(1-\alpha)^n \frac{de^{-E/RT}}{dt} + Ae^{-E/RT}\frac{d(1-\alpha)^n}{dt}\right]$$
$$= \frac{d\alpha}{dt}\left[\frac{E\frac{dT}{dt}}{RT^2} - An(1-\alpha)^{n-1}e^{-E/RT}\right] \tag{3}$$

Boundary conditions

$$\frac{d}{dt}\left[\frac{d\alpha}{dt}\right] = 0 \tag{4}$$

Obtain

$$\frac{E\frac{dT}{dt}}{RT_P^2} = An(1 - \alpha_p)^{n-1}e^{-E/RT} \tag{5}$$

Studies show that $n(1 - \alpha_P)^{n-1}$ does not correlate with β, (5) is changed to:

$$\frac{E\beta}{RT_P^2} = Ae^{-E/RT_P} \tag{6}$$

Taking the logarithm

$$\ln\left\{\frac{\beta}{T_P^2}\right\} = \ln\frac{AR}{E} - \frac{E}{R}\frac{1}{T_P} \tag{7}$$

where T_P (k) is the peak temperature, E (kJ mol^{-1}) is the activation energy and R (J mol^{-1} k^{-1}) is the ideal gas constant. $\ln(\beta/T_P^2)$ shows a linear relationship to $(1/T_P)$ in the Fig. 8a, which is a straight line and from which E can be calculated. In addition, the relationship between EG content and E conforms to the Boltzmann model:

$$y = A_2 + (A_1 - A_2)/(1 + \exp(x - x_0)/dx) \tag{8}$$

Here, the curve fitting parameters are: $A_1 = 360.96031$, $A_2 = 37634.497$, $x_0 = 87.63054$, $dx = 16.37116$ and $R^2 = 0.99934$, as shown in Fig. 8b. The parameters obtained from Table 2 show that the value of E for DA/EG-PCMs increases with increase in EG content. This indicates that the inhibition of the thermal diffusion of DA brought about by EG increases, as a result of which, the phase change is significantly hindered. Moreover, When the EG content exceeds 10 mass%, E increases rapidly, and the E of DA/EG-PCMs with 20 mass% EG reaches
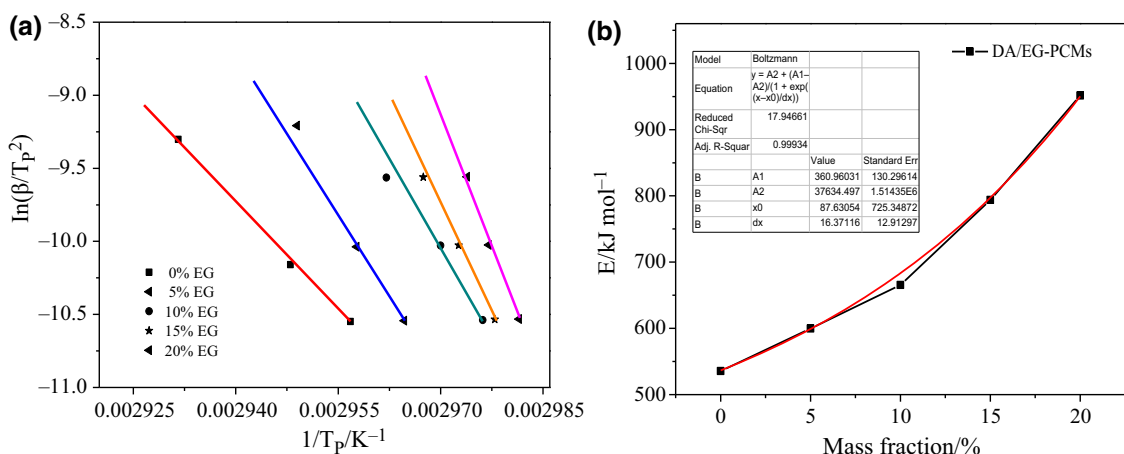

Fig. 8 Plot ln (β/T_P^2) versus $1/T_p$ and activation energy

Table 2 Thermal properties parameters of DA/EG-PCMs with different mass fraction of EG

EG/mass%	B/K min^{-1}	T_p/K	T_0/K	H_m/J g^{-1}	ΔH_c/J g^{-1}	E/kJ mol^{-1}	R^2	G/%
0	3	312.1	307.8	177.0	177.0	535.6	0.9951	100
	5	312.9	308.5					
	8	313.7	309.4					
5	3	311.4	306.6	166.3	168	599.8	0.9650	98.9
	5	312.1	307.4					
	8	313.0	308.2					
10	3	310.5	305.8	153.1	159.3	685.6	0.9825	96.1
	5	311.2	306.5					
	8	312.1	307.1					
15	3	309.3	305.1	131.4	150.5	793.9	0.9941	87.3
	5	310.1	305.9					
	8	311.0	306.6					
20	3	308.9	304.4	111.5	141.6	951.3	0.9915	78.7
	5	309.5	305.2					
	8	310.3	306.0					

$G = (H_m/\Delta H_c) \times 100\%$

951 kJ mol^{-1}. Therefore, it is clear that EG, which is an inorganic heterogeneous phase, significantly influences the phase change behavior of DA in the composite. These results show that, only when the content of EG is below 10 mass%, minor negative effects on the thermo physical properties are observed for the phase change in the system.

Thermal conductivity of DA/EG-PCMs

Thermal conductivity

Figure 9 shows the thermal conductivity and the increase in the thermal conductivity of DA/EG-PCMs with EG content. It can be seen that the thermal conductivity of pure DA is as low as 0.4128 W m^{-1} K^{-1}, and increases nearly linearly with EG content. The linear fit is represented by the equation $Y = 0.681 + 0.279X$ with a correlation coefficient $R^2 > 0.98$. The thermal conductivity reaches 6.2321 W m^{-1} K^{-1} when the EG content is 20 mass%, which enhances the thermal conductivity of pure DA by a factor of 15, demonstrating that the thermal conductivity of DA/EG-PCMs increases greatly with the addition of EG.
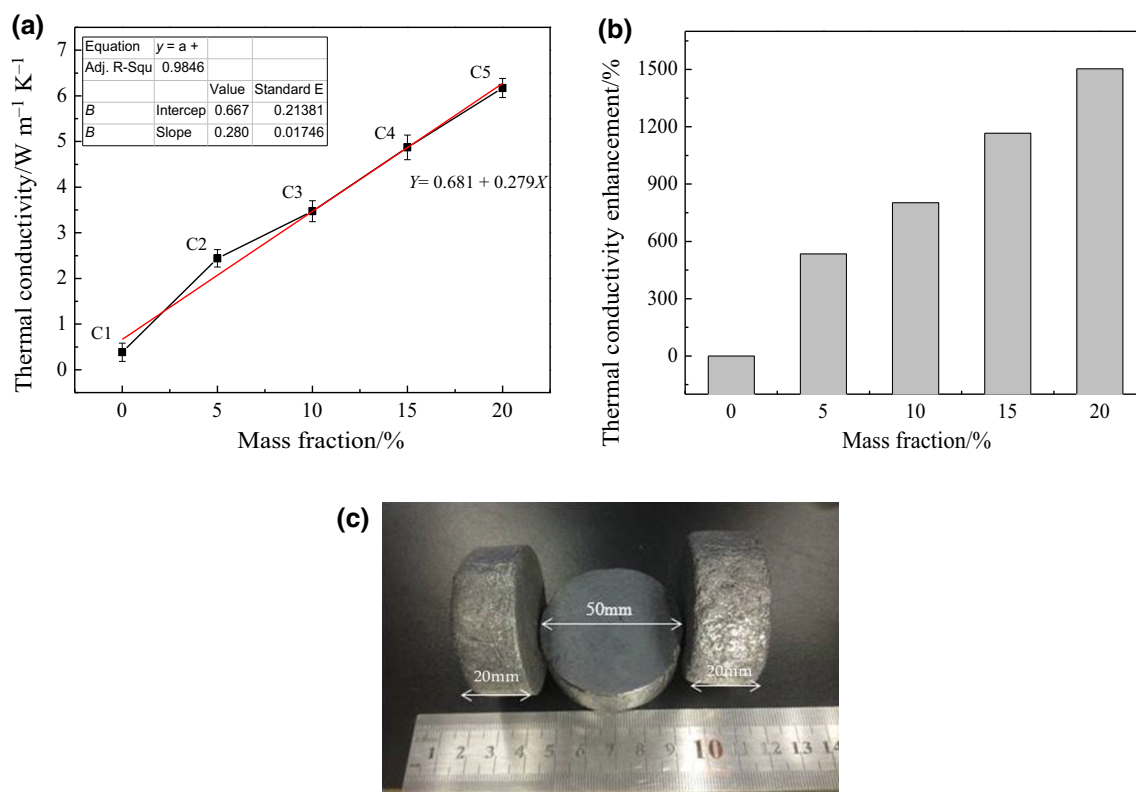
The heat transfer model

To better describe the heat transfer in DA/EG-PCMs, a model for this process has been described (Fig. 10). It can be seen that DA is a molecular crystal where the heat transfer is through the radiation of heat by molecular vibration. Hence, heat transfer is very slow due to its large thermal resistance. However, when it is in liquid phase the heat transfer in DA takes place by heat convection by Brownian motion. In EG, the heat conduction mainly depends on the phonon thermal conductivity, which means its rate is high due to the thermal motion of molecules and the low thermal resistance. When the mass fraction of EG in DA/EG-PCMs is low, the amount of DA exceeds the saturated adsorption capacity of EG, and therefore, the vermicular structure presents dispersive to be surrounded by the DA matrix to form the architecture like "Sea-Island". It is unable to form the whole heat transfer path with EG framework [28]. With increase of EG content, a perfect heat transfer network is formed by the overlapping and entangling of EG (Fig. 10c). This effect can improve the heat transfer, and speed up the rate, so that the capacity of heat transfer increased significantly.

Thermal stability of DA/EG-PCMs

Figure 11 shows the thermal stability of DA/EG-PCMs with (a) the TG, (b) the DTG, and (c) the DSC curves. It is observed that the removal of pure DA starts around 120 °C, and a mass loss of nearly 100% is achieved at 225 °C. In the TG curve, the mass loss in the temperature range 110–220 °C is attributed to the decomposition of the molecular chains of DA in the DA/EG-PCMs. This mass loss is in accordance with the DA content in DA/EG-PCMs [29]. In the DTG curve, the rate of decomposition of DA in DA/EG-PCMs depends on the EG content and this value tends to decrease with the increase of EG content. This result indicates that the maximum decomposition temperature and decomposition rate of pure DA are higher than for DA/EG-PCMs.

Fig. 9 **a** The thermal conductivity of DA/EG-PCMs **b** the thermal conductivity enhancement **c** photos of DA/EG-PCMs
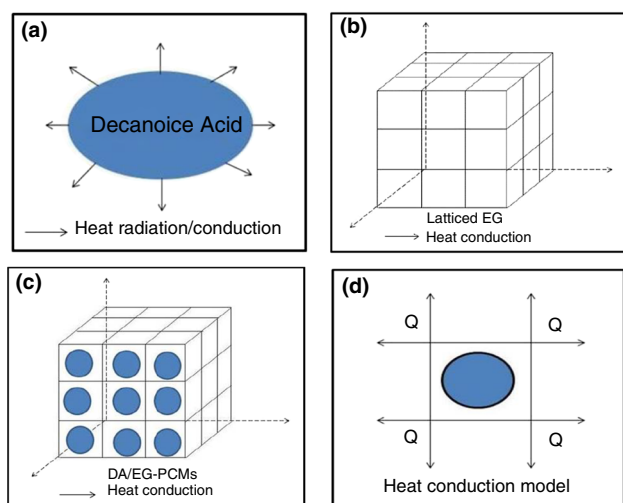

Fig. 10 The model for heat transfer of DA/EG-PCMs

The DSC curve of DA/EG-PCMs is characterized by two endotherms, the first corresponding to the solid–liquid phase change ($t1$) and the second to the decomposition of DA ($t2$). With increasing EG content, these two endotherms shift to lower temperatures. Firstly, the thermal conductivity of DA/EG-PCMs increases with the addition of EG. Hence, it can absorb sufficient heat at a relatively lower temperature to melt and decompose. Secondly, DA is

a molecular crystal with intermolecular hydrogen bonds. With the addition of EG, hydrogen bonds form between the molecular chains in DA and the functional groups in EG, resulting in a reduced number of hydrogen bonds among the DA molecules, as shown in Fig. 12. For molecular crystals, the melting and boiling points decrease with the decrease in the number of hydrogen bonds. Thirdly, DA can evaporate at high temperatures and the inhibition effect of EG weakens in the gas phase. Although the mass loss interval and the peak temperature of decomposition decrease gradually with the addition of EG, DA/EG-PCMs can also exhibit excellent thermal stability used in the control of temperature in low-to-medium temperature environment (<80 °C).

The capacity of charging and discharging heat of DA/EG-PCMs

The heat charging and discharging capacity curves for DA/EG-PCMs are shown in Fig. 13; the overall trends can be divided into three phases. At stage a1, the sample temperatures increase at different rates under constant temperature (water bath at 60 °C). Due to its high thermal resistance and low thermal conductivity, the temperature of $C1$ increases slowly while the temperatures of the other four samples increase at a relatively higher speed. This is
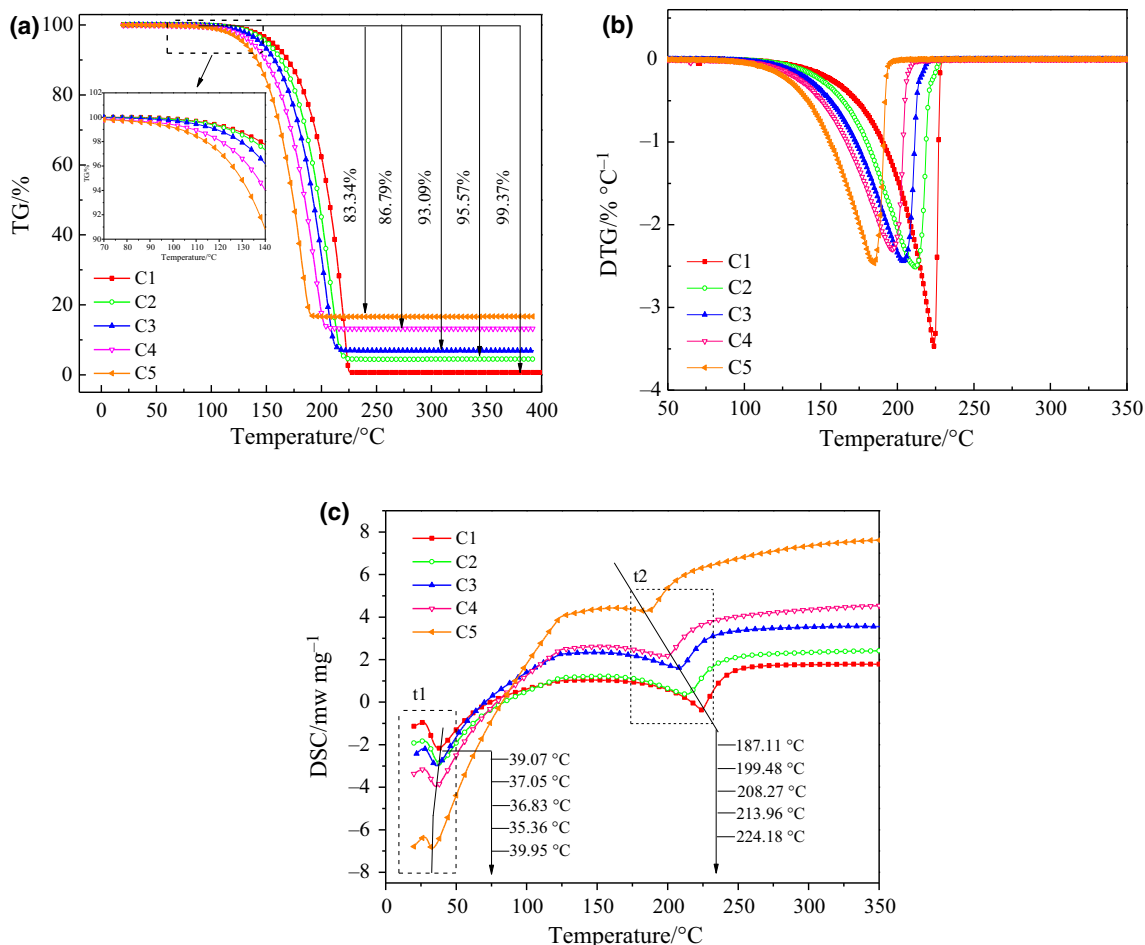
Fig. 11 Thermal analysis of DA/EG-PCMs
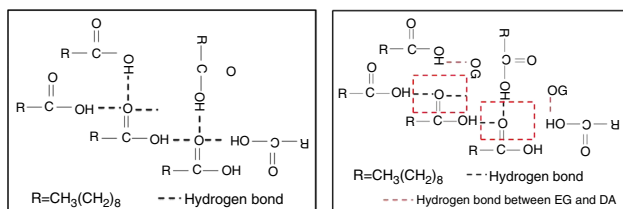
Fig. 12 Hydrogen bonding in **a** DA **b** DA/EG-PCMs

the stage representing sensible heat storage without phase change. At stage a2, DA melts to absorb heat and the rate of temperature rise slows down, $\lim_{t=t_0}^{t} \partial T/\partial t_{sample} \neq 0$, $\lim_{t=t_0}^{t} \partial T/\partial t_{reference} \neq 0$, ($t_0$ is the time where the phase change begins). In addition, a constant temperature plateau appears, the length of which reduces with increase in EG content. This is due to the fact that the thermal conductivity increases, and the phase change temperature and latent heat reduce, leading to a lower temperature difference between phase change and the heating surface. As a result, less heat is absorbed during the process of phase change. This state

represents sensible and latent heat storage. At stage a3, the temperature rises more rapidly and the phase change terminates to give rise to sensible heat storage in molten DA. Compared to the other four samples, the temperature of $C1$ rises at a higher rate. Since the heat that is absorbed from the external source cannot be transmitted to the internal, it can only be stored in the form of sensible heat (a1). As the temperature of the liquid DA rises, its density decreases as a result of which it moves upwards under the action of buoyancy. The rates of melting and temperature rise accelerate under the influence of the rising heat flow. The temperatures of the other samples increase more slowly, mainly because the DA in DA/EG-PCMs is fixed by EG. Therefore, the macro flow of the liquid is restricted, and the natural convection of the composite system is remarkably reduced. Eventually, the slopes of the five curves are 0, $\lim_{t=t_1}^{t} \partial T/\partial t_{sample} = 0$, $\lim_{t=t_1}^{t} \partial T/\partial t_{reference} = 0$. The temperatures of the samples and that of the water bath reach a state of equilibrium. The observed trends after dipping the samples in the water bath at room temperature can also be divided into three phases to contrast with the storage curve,
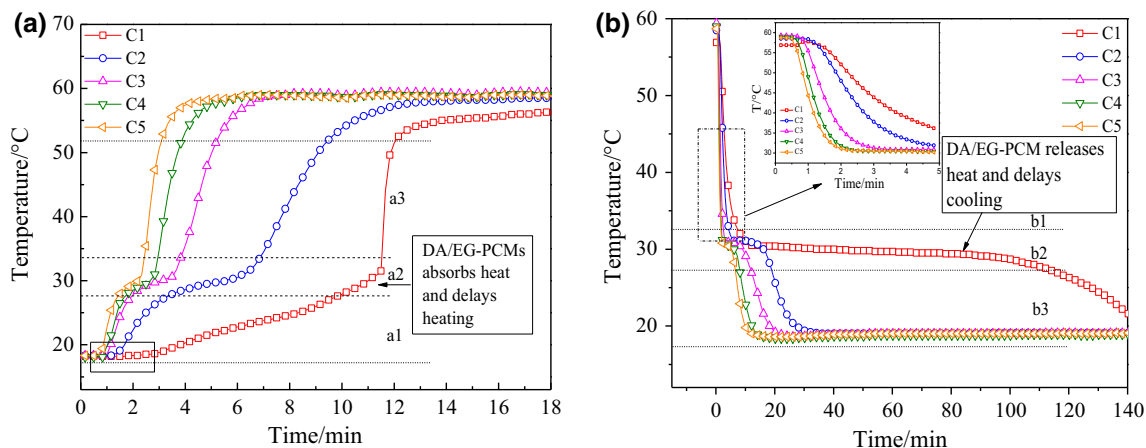
Fig. 13 Heat charging and discharging capacity curve of DA/EG-PCMs

and the molten DA is frozen to release heat. Finally, the temperature remains constant.

During the heating process (Fig. 13a), it takes 13 min for pure DA to raise its temperature from room temperature (~20 °C) to the temperature plateau of 60 °C but this time is only 10 min, 6 min, 4 min and 3 min for C2, C3, C4, and C5. During the cooling process (Fig. 13b), the temperature reaches a plateau around 20 °C after 30, 20, 18 and 17 min for C2, C3, C4 and C5, respectively, whereas for pure DA, this time interval is around 140 min. Compared with pure DA, the DA/EG-PCMs reaches the temperature plateau in a shorter time, indicating that the thermal storage/release rates are increased in these samples. Therefore, the heat from the external environment can be evenly transmitted to the internal due to the presence of EG with a high thermal conductivity which can effectively reduce the thermal resistance. In conclusion, the addition of EG can effectively improve the melting transition, the capacity of charging and

discharging heat, and the thermal efficiency of DA/EG-PCMs [30].
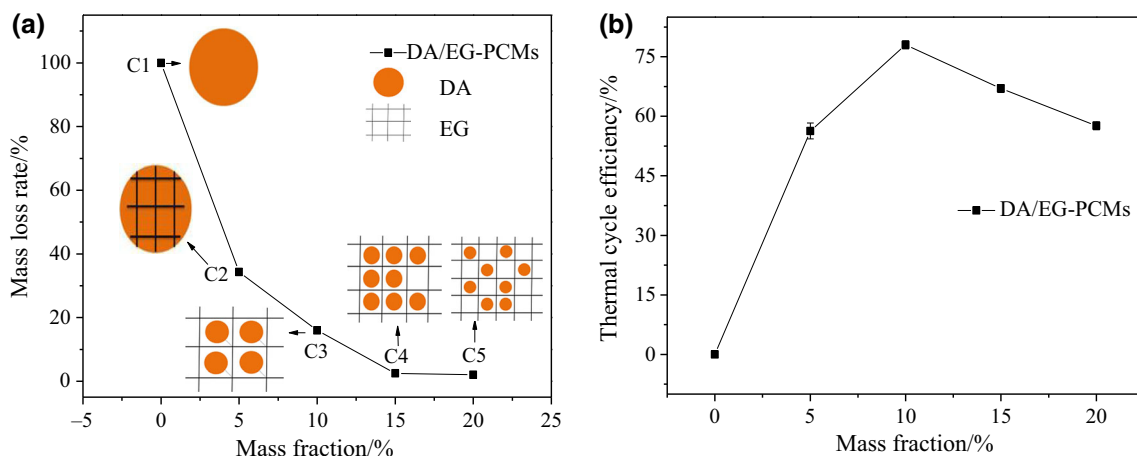
Thermal cycling stability of DA/EG-PCMs

Mass loss rate

In order to more clearly describe the changes in performance of DA/EG-PCMs after the thermal cycle, this paper defines K as the mass loss rate:

$$K = \frac{M_1 - M_2}{M_1} \times 100\% \tag{9}$$

M_1 is the mass before the cycle and M_2 is the mass after the cycle. The thermal cycle efficiency (E_e) can be calculated from the experimental results and according to Eqs. 10.

$$E_e = \frac{\Delta H_{m,1}}{\Delta H_{m,DA}} \times 100\% \tag{10}$$

Fig. 14 The mass and thermal cycle efficiency changes in DA/EG-PCMs during the thermal cycle

where $\Delta H_{m,1}$ is the latent heat of DA/EG-PCMs after cycling and $\Delta H_{m,DA}$ is the latent heat of pure DA.

Figure 14 shows the changes in mass and thermal cycle efficiency of samples before and after thermal cycling between 25 and 100 °C, respectively. It can be seen that the mass loss rate is 34% (a high loss), and the thermal cycle efficiency is low when the content of EG is 5 mass%. Here, upon heating, the DA that is not encapsulated by EG melts
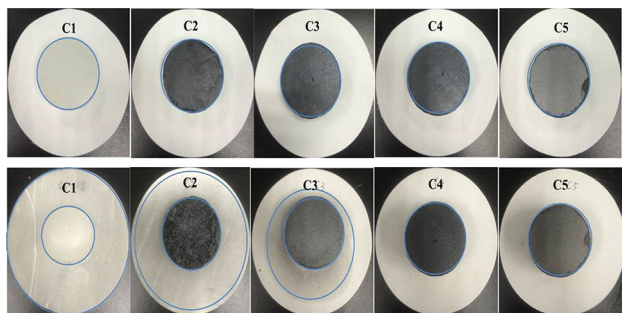

Fig. 15 The thermal cycling stability of DA/EG-PCMs

and starts to flow. When the content of EG reaches 10 mass% and higher, there is basically no loss of mass, and the separation and delamination between EG and DA disappears. This phenomenon is attributed to the confinement effect of EG on the crystallization of the encapsulated DA, as shown in Fig. 14a. In addition, as shown in Fig. 14b, the thermal efficiency of cycling first increases, and then decreases, and reaches a maximum value at about 10 mass%. This is attributed to the fact that DA exposed on the surface melts and separates from EG when the EG content is low and the thermal cycle efficiency decreases due to the reduction in DA content. Moreover, with increase in EG content, the microscopic flow of molten DA is limited, so that the thermal cycle efficiency of DA/EG-PCMs is improved [31]. Figure 15 shows the photographs of pure DA and the DA/EG-PCMs before and after the thermal cycle. As seen from the photographs, pure DA completely melts into a liquid after the thermal cycle, whereas, the DA/EG-PCMs retain its form during the whole heating process. The above analysis confirms that the shell formed by EG s provides mechanical strength for
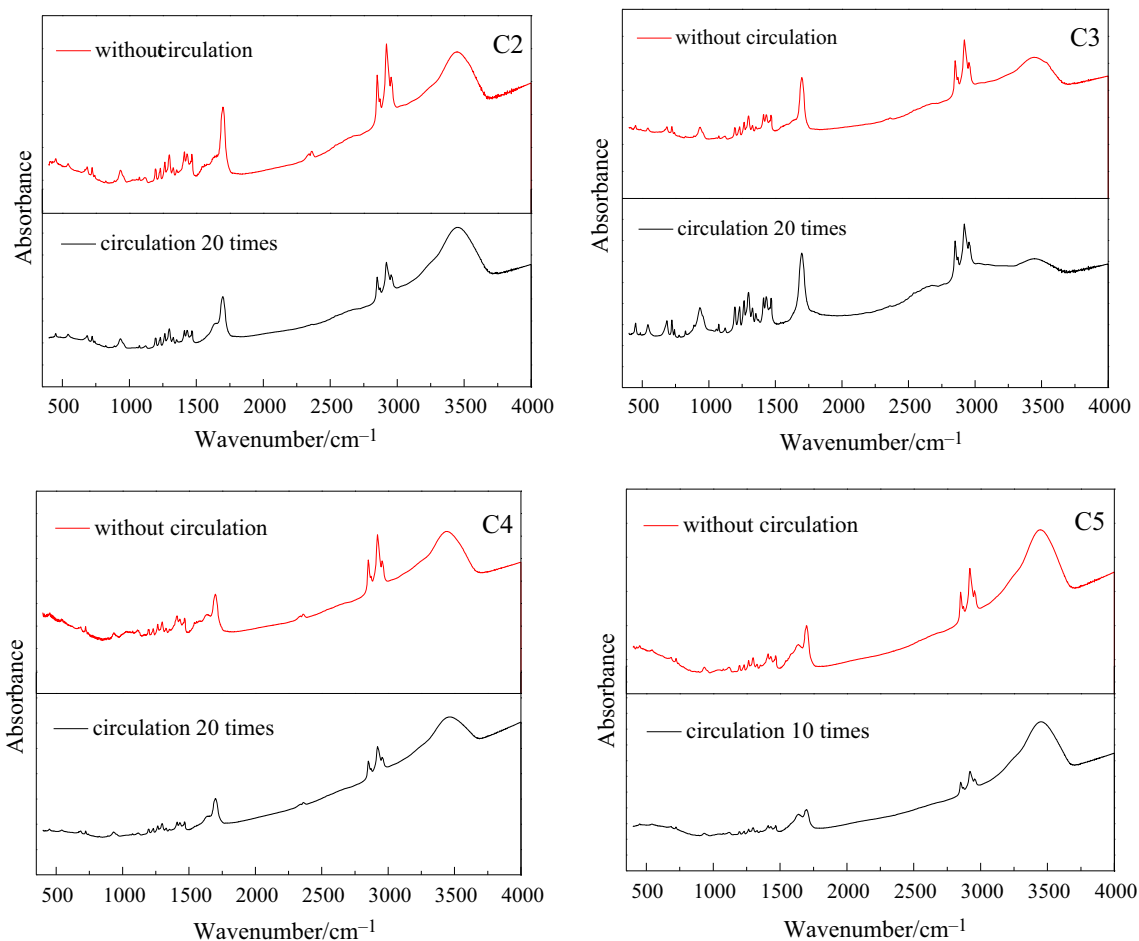
Fig. 16 FT-IR spectra of DA/EG-PCMs before and after thermal cycling
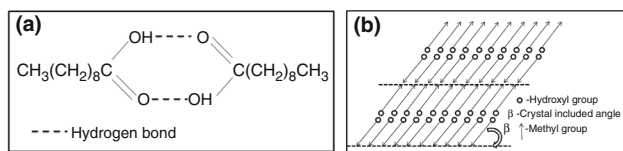
Fig. 17 **a** Bilayer arrangement of DA **b** Molecular layer of DA in the solid

the microencapsulated composite and prevents the seepage of the melted DA. Therefore, the DA/EG-PCMs with 10 mass% EG present excellent thermal stability and efficiency.

Infrared spectrum analysis

Figure 16 shows the IR spectra of DA/EG-PCMs before and after thermal cycling. The results obtained from Fig. 16 show that the infrared spectra are basically the same. Two intense absorption peaks at 2925 and 1465 cm^{-1} are present, which are attributed to C-H stretching and C-H in-plane bending vibrations respectively. The infrared spectra also show absorption peaks at 1430 and 940 cm^{-1} attributed to -OH in-plane and out of plane bending vibrations. A peak at 1716 cm^{-1} corresponding to C=O stretching vibration is also observed. In addition, some small shifts in the characteristic absorption peaks indicate physical interactions between EG and DA. The absorption peaks are in good agreement with the FT-IR spectra of the samples before cycling, no new functional groups or chemical species are produced in the process of thermal cycling, and the molecular structure of DA remains unchanged. In addition, the two association structure in the way of bilayer arrangement forms between the molecules of DA (Fig. 17a), and the hydroxyl and methyl end-groups of DA are all in the parallel plane (Fig. 17b). When the temperature rises, the crystal dissociates along the face between methyls. Further melting increases the association between the molecules and this effect is so strong that it cannot be easily destroyed in the process of thermal cycling. Moreover, the interaction between the methyls remains unchanged and is not affected by the number of cycles. Therefore, DA/EG-PCMs retain a stable molecular structure and high thermal efficiency even after cycling, and maintain good and long-term thermal stability.

Conclusions

The following conclusions can be drawn from our investigation:

1. The decanoic acid/expanded graphite composite phase change materials (DA/EG-PCMs) are prepared by the melt-blending method with expanded graphite (EG) as the carrier material and decanoic acid (DA) as the phase change material. The DA/EG-PCMs form a composite stabilized by surface adsorption and micropore binding, without the formation of chemical bonds.

2. The DA/EG-PCMs are spherical with a smooth surface, low particle sizes, and good dispersions, which facilitates their mixing with other granular materials.

3. DA/EG-PCMs can form a perfect heat transfer network based on the EG framework that enhances the thermal conductivity. The phase change temperature is reduced, and the time to charge and discharge heat is reduced, leading to improved thermal efficiency.

4. The calculated activation energies indicate that EG inhibits the thermal diffusion of DA, which increases the thermal stability. Due to the micropore binding, surface adsorption and the association structure, DA/EG-PCMs exhibit a good thermal cycling stability and meet the requirements of long-term services.

5. Based on a comprehensive analysis, it can be concluded that, the optimal content of EG is ~ 10 mass%. The thermal conductivity of DA/EG-PCMs is ~ 3.4721 W m^{-1} K^{-1}. The heat storage time is shortened by ~ 53%, the phase change temperature is 34.9 °C, and the latent heat is 153.1 J g^{-1}. In view of these properties, the DA/EG-PCMs can well meet the requirements for low-to-medium temperature controllers.

References

1. Cheralathan M, Velraj R, Renganarayanan S. Heat transfer and parametric studies of an encapsulated phase change material based cool thermal energy storage system. J Zhejiang Univ Sci A. 2006;7(11):1886–95.
2. Ho CJ, Gao JY. Preparation and thermophysical properties of nanoparticle-in-paraffin emulsion as phase change material. Int Commun Heat Mass Transf. 2009;36(5):467–70.
3. Ince S, Seki Y, Ezan MA, et al. Thermal properties of myristic acid/graphite nanoplates composite phase change materials. Renew Energy. 2015;75:243–8.
4. Lin Y, Chen HL. Thermal analysis and adiabatic calorimetry for early-age concrete members. J Therm Anal Calorim. 2015;122(2):937–45.
5. Varol Y, Koca A, Oztop HF, et al. Forecasting of thermal energy storage performance of phase change material in a solar collector using soft computing techniques. Expert Syst Appl. 2010;37(4):2724–32.
6. Qiu X, Lu L, Zhang Z, et al. Preparation, thermal property, and thermal stability of microencapsulated n-octadecane with poly (stearyl methacrylate) as shell. J Therm Anal Calorim. 2014;118(3):1441–9.
7. Zheng Y, Barton JL, Tuzla K, et al. Experimental and computational study of thermal energy storage with encapsulated NaNO 3 for high temperature applications. Sol Energy. 2015;115:180–94.

8. Zhang GH, Zhao CY. Thermal property investigation of aqueous suspensions of microencapsulated phase change material and carbon nanotubes as a novel heat transfer fluid. Renew Energy. 2013;60:433–8.

9. Zhao L, Wan T, Yang X, et al. Effects of kaolinite addition on the melting characteristics of the reaction between phosphogypsum and CaS. J Therm Anal Calorim. 2015;119(3):2119–26.

10. Silva LFO, Hower JC, Izquierdo M, et al. Complex nanominerals and ultrafine particles assemblages in phosphogypsum of the fertilizer industry and implications on human exposure. Sci Total Environ. 2010;408(21):5117–22.

11. Warzoha RJ, Fleischer AS. Improved heat recovery from paraffin-based phase change materials due to the presence of percolating graphene networks. Int J Heat Mass Transf. 2014;79:314–23.

12. Wu SY, Tong X, Nie CD, et al. The effects of various carbon nanofillers on the thermal properties of paraffin for energy storage applications. J Therm Anal Calorim. 2016;124(1):181–8.

13. Trigui A, Karkri M, Krupa I. Thermal conductivity and latent heat thermal energy storage properties of LDPE/wax as a shape-stabilized composite phase change material. Energy Convers Manag. 2014;77:586–96.

14. Wang L, Meng D. Fatty acid eutectic/polymethyl methacrylate composite as form-stable phase change material for thermal energy storage. Appl Energy. 2010;87(8):2660–5.

15. Li H, Ji X, Leng C, et al. Thermal performance of expanded graphite/Na$_2$S$_2$O$_3$·5H$_2$O phase change energy storage composite. Acta Mater Compos Sinic. 2016;33(12):2941–51.

16. Sarı A, Sarı H, Önal A. Thermal properties and thermal reliability of eutectic mixtures of some fatty acids as latent heat storage materials. Energy Convers Manag. 2004;45(3):365–76.

17. Sarı A. Eutectic mixtures of some fatty acids for latent heat storage: thermal properties and thermal reliability with respect to thermal cycling. Energy Convers Manag. 2006;47(9):1207–21.

18. Babaei H, Keblinski P, Khodadadi JM. Thermal conductivity enhancement of paraffins by increasing the alignment of molecules through adding CNT/graphene. Int J Heat Mass Transf. 2013;58(1):209–16.

19. Zhang P, Hu Y, Song L, et al. Effect of expanded graphite on properties of high-density polyethylene/paraffin composite with intumescent flame retardant as a shape-stabilized phase change material. Sol Energy Mater Sol Cells. 2010;94(2):360–5.

20. Tang F, Cao L, Fang G. Preparation and thermal properties of stearic acid/titanium dioxide composites as shape-stabilized phase change materials for building thermal energy storage. Energy Build. 2014;80:352–7.

21. Zhong LM, Yang M, Luan L. Preparation and properties of paraffin/SiO$_2$ composite phase change materials. Chin J Eng. 2015;37(7):936–41.

22. Zhang XR, Zhu DS, Gao JW. Study on thermal properties of graphite/paraffin composites as phase change heat storage materia. Chin J Mater Res. 2010;24(3):332–6.

23. Li JF, Lu W, Zeng YB, et al. Simultaneous enhancement of latent heat and thermal conductivity of docosane-based phase change material in the presence of spongy graphene. Sol Energy Mater Sol Cells. 2014;128:48–51.

24. Yang H, Mao J, Feng J. Investigation on preparation and performance of paraffin/silicon dioxide composite phase change materials. Mater Rev. 2010;24(15):278–80.

25. Yang JG, Wu CP. Morphology and X-ray photoelectron spectroscopy of expanded graphite. J Mater Sci Eng. 2007;25(2):294–7.

26. Sarı A, Karaipekli A. Thermal conductivity and latent heat thermal energy storage characteristics of paraffin/expanded graphite composite as phase change material. Appl Therm Eng. 2007;27(8):1271–7.

27. Huang X, Cui YD, Yin GQ, Zhang BN. Preparation and phase transformation kinetic of organic modified montmorillonite based composite phase change material. Mater Rev. 2015;29(8):63–6.

28. Zhang WP, Tong F, Xing YS. Experimental study and prediction model of thermal conductivity of concrete. J Build Mater. 2015;18(2):183–9.

29. Zhu FR, Zhang L, Zeng JL, et al. Preparation and thermal properties of palmitic acid/polyaniline/copper nanowires form-stable phase change materials. J Therm Anal Calorim. 2014;115(2):1133–41.

30. Yu H, Gao J, Chen Y, et al. Preparation and properties of stearic acid/expanded graphite composite phase change material for low-temperature solar thermal application. J Therm Anal Calorim. 2016;124(1):87–92.

31. Zhang H, Huang XJ, Liu XY. Optimization for preparation of phase change and humidity control composite materials of hexadecanol-palmitic acid-lauric acid/SiO$_2$. Chin J Mater Res. 2015;29(9):671–7.